Redox Properties of Structural Fe in Clay Minerals: 4. Reinterpreting Redox Curves by accounting for Electron Transfer and Structural Rearrangement Kinetics

Vineeth Pothanamkandathil[a], Anke Neumann[b], Aaron Thompson[c] and Christopher A. Gorski[a,*]

[a] Department of Civil and Environmental Engineering, The Pennsylvania State University, University Park, PA 16802, USA

[b] Paul Scherrer Institut, 5232 Villigen, Switzerland

[c] Department of Crop and Soil Sciences, The University of Georgia, Athens, GA 30602, USA

*Corresponding author: Email: gorski@psu.edu; Tel: +1 814-865-5673

KEYWORDS: Iron, Smectites, Redox-potential, Kinetics, Equilibrium, Electrochemistry, Hysteresis.

ABSTRACT

Iron-bearing smectite clay minerals can act as electron sources and sinks in the environment. Previous studies using mediated electrochemical analyses to determine the reduction potential (E_H) values of smectites observed that the relationship between the structural $Fe^{2+}_{(s)}/Fe_{Total}$ ratio in the smectite and E_H varied based on the redox history of the smectite. We hypothesize that this behavior, referred to as redox hysteresis, results from the smectite particles not equilibrating with the applied E_H over the course of the experiment (~30 minutes). To test this hypothesis, we developed a model incorporating interfacial electron transfer kinetics and charge redistribution within the particle to simulate the mediated electrochemical experiments from previous studies. The simulated redox curves accurately matched the previously reported experimental redox

curves of the smectite SWa-1, demonstrating that longer equilibration periods led to a decrease in redox hysteresis. We validated this experimentally by measuring the redox curve of SWa-1 after an equilibration period of at least 12 hours. Furthermore, we extended the simulations to three other smectites (NAu-1, NAu-2, and SWy-2) and extracted their respective thermodynamic and kinetic parameters. This work offers a framework for interpreting and modeling redox reactions on clay surfaces, along with key parameters for four commonly studied smectites.

SHORT SYNOPSIS STATEMENT

This study provides a mechanistic model for interpreting and modeling redox reactions involving smectite clay minerals.

Graphic for Manuscript

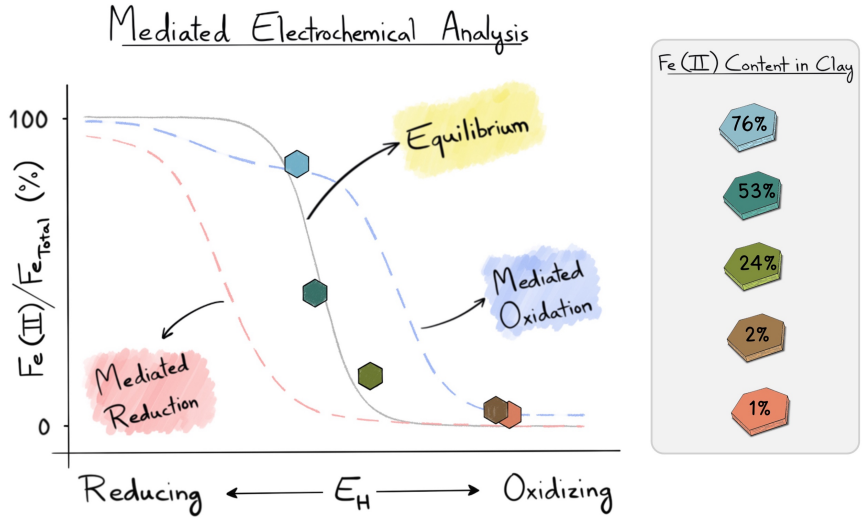

INTRODUCTION

Iron-bearing clay minerals can serve as electron donors/acceptors in the environment, with structural iron participating in redox reactions with microorganisms, nutrients, and environmental contaminants.[1-13] Smectite-type clay minerals have received particular attention in the scientific literature because most or all of their structural iron is capable of being reduced and oxidized under environmentally relevant conditions.[4-7, 14-20] In smectites, the structural iron is largely preserved due to the silicate tetrahedral sheets sandwiching the Fe-bearing octahedral sheet and the mineral compensating for changes in charge via reversible uptake of cations and/or protons:

$$\mathrm{Fe}^{3+}_{(s)} + \mathrm{e}^{-} + x\mathrm{H}^{+}_{(aq)} + y\mathrm{Cat}^{+}_{(aq)} = \mathrm{Fe}^{2+}_{(s)} - \mathrm{H}^{+}_{x(s)}\mathrm{Cat}^{+}_{y(s)} \quad (1)$$

in which Cat^{+} is a generic cation and the electron comes from an external donor and $x + y = 1$. Prior efforts have established that the rates and extents of redox reactions involving structural Fe in smectites depend on the structural $\mathrm{Fe}^{2+}_{(s)}/\mathrm{Fe}_{\mathrm{Total}}$ ratio, which controls both the reduction potential (E_{H}) of the mineral and the number of reactive sites.[3-7, 14, 15, 17, 18, 21-28] However, attempts to quantify E_{H} values of structural Fe in smectites have faced challenges.

Prior work by our group used mediated electrochemical experiments to determine the relationships between the $\mathrm{Fe}^{2+}_{(s)}/\mathrm{Fe}_{\mathrm{Total}}$ ratio and E_{H} for four purified naturally-occurring smectites (SWy-2, SWa-1, NAu-1, and NAu-2).[14, 21, 22] In the mediated electrochemical experiments, soluble redox shuttles were used to facilitate electron transfer between smectite particles suspended in an electrolyte and a working electrode.[14, 21, 22, 28-30] In one set of experiments, a known amount of a smectite that was initially fully oxidized ($\mathrm{Fe}^{2+}_{(s)}/\mathrm{Fe}_{\mathrm{Total}} \approx 0$) was spiked into a solution poised at an

E_H value, and the extent of reduction was quantified by integrating the resulting current response in a method referred to as mediated electrochemical reduction (MER). In a second set of experiments, a known amount of reduced sample was oxidized to different extents in a method referred to as mediated electrochemical oxidation (MEO).[14, 21, 22] The final $Fe^{2+}_{(s)}/Fe_{Total}$ values were then plotted against the applied E_H values to produce redox profiles for the smectites.[21, 22]

A critical finding from our prior work was that the measured redox curves exhibited two types of hysteresis (i.e., the $Fe^{2+}_{(s)}/Fe_{Total}$ ratio to E_H relationships differed depending on the history of the smectite).[21, 22] Specifically, the redox curve obtained from the mediated electrochemical experiments differed depending on whether the smectite was initially (*i*) unaltered, (*ii*) reduced using dithionite, or (*iii*) re-oxidized after dithionite reduction.[21, 22] The first type was only observed between the redox curve of a "native" (i.e., unaltered) smectite and a "re-oxidized" smectite (i.e., reduced using sodium dithionite and subsequently re-oxidized using hydrogen peroxide).[21, 22] The difference in the redox curves was relatively small and was attributed to the irreversible changes that occur during dithionite reduction of smectites.[13, 21, 22] The second—more significant—type of hysteresis appeared when comparing the initially reduced and re-oxidized smectites.[21, 22] Specifically, the redox curves of the reduced and re-oxidized smectite differed considerably.[21, 22] This second type of hysteresis was reproducible over multiple redox cycles and was speculated to be due to the formation of metastable Fe states on the clay surface.[21, 22] A consequence of the observed hysteresis was that we could not identify a singular standard reduction potential (E_H^0) value for a given smectite.[21, 22]

We now suspect that the observed redox hysteresis was due to the system not reaching equilibrium over the experimental time scale. Evidence for this suspicion comes from studies performed on other intercalating materials (e.g., Prussian blue analogs, $LiMnO_2$, and $LiFePO_4$) often used for energy storage and electrochemical ion separation.[31-42] Here, intercalation refers to the reversible insertion of a cation into the particle without an overt change to the crystal structure. The charge transfer process for intercalation materials involves (at least) two steps: (1) reduction of a structural redox-active site accompanied by cation or proton uptake at the mineral-electrolyte interface and (2) cation or proton diffusion from the surface of the mineral into its bulk structure to dissipate the concentration gradient created by step 1.[32-34, 43-45] If an experiment performed on an intercalating material is short relative to the time it takes for these processes to reach an equilibrium state, the collected data appears irreversible.[44-48] The mediated electrochemical experiments performed on the smectites occurred over 30 minutes, but other experiments done with probe compounds suggest the time needed to reach equilibrium may be several days.[4, 6, 7, 21, 22, 49] Recent experiments have also suggested temporary $Fe^{2+}_{(s)}/Fe_{Total}$ gradients within a smectite crystal lattice after a surface redox reaction and indicated that the dissipation of the concentration gradient may take multiple days.[50, 51]

The central hypothesis of this paper was that the existing electrochemical data for smectites could be reproduced with a mechanistically appropriate model that captures interfacial electron transfer kinetics and charge dissipation within the crystal structure to quantify thermodynamic and kinetic properties of the smectites. To test this, we developed a model that described the reaction between the redox mediator and the smectite particle during a mediated electrochemical reaction. In this model, the rate of charge transfer between the mediator and the

edge of the smectite particle was determined as a function of the E_H value and the Nernst-Frumkin equation.[33, 34, 52, 53] We focused on the edge sites, as previous studies demonstrated that charge transfer predominantly occurs at edges at pH values ≥ 7.[18, 54] The subsequent migration of charged species from the edge into the bulk of the smectite particle was modeled as a one-dimensional diffusion process. The diffusive transport affected the rate at which the E_H value of the clay surface changed over time.[34, 53, 55] We used a one-dimensional approach because it captured the dissipation of the $Fe^{2+}_{(s)}/Fe_{Total}$ gradient within the smectite particle effectively, while avoiding the additional computational demands of a higher-dimensional model. Note that a more complex, multidimensional model would be needed to accurately describe charge transfer between surface basal sites and structural iron atoms. Using the model, we fit the redox profiles collected by Gorski et al. (2013) to determine the E_H^0 value of four naturally occurring smectites (SWy-2, SWa-1, NAu-1, and NAu-2).[22] These four smectites were selected in our previous studies due to the thorough documentation of their physical and chemical properties and their commercial availability from the Clay Minerals Society.[14, 21, 22] To further validate our hypothesis that redox hysteresis is a manifestation of apparent irreversibility, we also performed mediated potentiometry on SWa-1 suspensions with different $Fe^{2+}_{(s)}/Fe_{Total}$ ratios. These suspensions were allowed to react with redox mediators overnight to determine if the redox curve generated from the measured E_H values fell within the redox curves previously collected by Gorski et al.[21, 22]

MATERIALS AND METHODS

All solutions were prepared by mixing reagents in deionized water (>18.2 MΩ·cm).

Anoxic conditions.

SWa-1 reduction and re-oxidation as well as mediated open-circuit measurements were conducted under anoxic conditions (<0.1 ppm O_2) in a glovebox (Unilab 2010, Mbraun GmbH, Germany) containing a N_2 atmosphere. All Solutions were sparged with ultra-high purity N_2 for one hour before being transferred into the glovebox. Plastic syringes, pipette tips, and glassware were evacuated overnight in the transfer chamber and equilibrated in the glovebox for several days before use.

SWa-1 reduction and re-oxidation experiments.

Ferruginous smectite (SWa-1, 12.6 % wt. Fe) was obtained from the Source Clay Minerals Repository (Purdue University, West Lafayette, IN). A SWa-1 clay suspension (10 $g \cdot L^{-1}$) with clay particles ≤ 0.5 μm in 0.1 M $NaClO_4$ was used for the reduction experiment. Detailed description on the preparation of the clay suspension was provided in our previous work.[14]

SWa-1 was reduced using the citrate-buffered dithionite method.[13] Briefly, 25 mL of the SWa-1 suspension was transferred to a glass bottle to which 50 mL of deionized water was added. This bottle was sparged with humidified ultra-high purity N_2 for an hour and transferred to the glovebox. To this bottle, 23.4 mL of 1 M $NaHCO_3$ (Fischer Chemical, 99.7%) and 1.6 mL of 0.3 M Na_3-citrate (EMD Chemicals Inc., 99%) were added. The suspension was stirred and heated to 70 °C, at which point sodium dithionite (Milapore Sigma Sigma-Aldrich, > 99%) was slowly added. The mass of sodium dithionite added was five times the mass of SWa-1 in suspension. The suspension was stirred vigorously at 70 °C overnight. The reduced SWa-1 suspension was transferred to a pre-washed and dried dialysis tube (molecular weight cutoff = 12– 14 kDa) and immersed in a 1 L solution of 0.1 M $NaClO_4$ (Fischer Sci, > 99%). The suspension was equilibrated

for 8 hours, after which the solution was replaced with fresh 0.1 M $NaClO_4$. This process was repeated four times. The suspension, with a final clay mineral concentration of ~2.5 $g \cdot L^{-1}$, was transferred to a glass bottle.

A previous study by our group demonstrated that nearly all the Fe atoms (>99%) in SWa-1 occupied octahedral sites and were redox-active, with an electron storage capacity of 2.20 $mmol \cdot g_{SWa\text{-}1}^{-1}$.[14] The approximate oxidant dose required to fully oxidize the dithionite-treated SWa-1 was calculated based on these values (**Section S1**). For the re-oxidation experiments, the reduced clay suspension was divided equally into five glass vials (20 mL suspension per vial). One vial was set apart as the "reduced" sample. Different volumes (30, 70, 110 and 140 μL) of 1.0 M H_2O_2 were added to each of the other four vials to re-oxidize the SWa-1 suspensions. A detailed account of the re-oxidation process is provided in **Section S1**. A portion (11 mL) of the clay suspension from each of the five vials was set aside for transmission ^{57}Fe Mössbauer spectroscopy analysis of the SWa-1 clay. Sample preparation and methodology for Mössbauer spectroscopy analysis is provided in **Section S2**. The remaining clay suspension (9 mL) was used for mediated open-circuit potential measurements.

Mediated potentiometry experiments.

A protocol previously used by our group to determine the standard reduction potential of hematite and goethite was modified to measure the E_H value of SWa-1 using mediated potentiometry.[25] Briefly, The background electrolyte used in the mediated potentiometry experiments was 0.1 M $NaClO_4$ buffered to pH 7.0 using 50 mM MOPS free acid (3-(N-morpholino)propanesulfonic acid, EMD Chemicals Inc., 99%) and sodium hydroxide. To 25 mL

of background electrolyte, 400 µL of SWa-1 clay suspension (~ 2.5 g·L^{-1}) and 50 µL of 10 mM redox mediator was added and allowed to react overnight (12-24 hours). The mediators used in this study were selected based on past work, ensuring that their standard reduction potentials at pH 7 spanned E_H values ranging between – 0.14 and + 0.43 V vs. SHE.[21, 22, 56] A table of redox mediators used along with their reduction potentials at pH 7 are provided in **Table S2**. After equilibration, the E_H value of the suspension was measured using a combined Pt-ring electrode (0.209 V vs. SHE, Metrohm, part 6.0451.100) for one hour. The Pt-ring electrode was calibrated using quinhydrone redox couple and the open-circuit potential measurements were logged using tiamo 2.3 (Metrohm). The Pt-ring electrode was immersed in 3 M KCl for at least three hours between consecutive E_H measurement experiments to minimize potential drift.[25]

Note that three different volumes (12.5, 25 and 50 µL) of the 10 mM redox mediator solution were tested when performing the mediated potentiometry experiments to ensure that specific adsorption of the mediator to the smectite did not influence the measured E_H value of the SWa-1 suspension.[22] No significant difference was found in the measured E_H values (i.e., within 25 mV of each other) across the three tested volumes.

THEORY AND MODEL DESCRIPTION

A redox reaction at a solid-water interface involves several steps: (*i*) diffusion of the redox-active compound to the solid surface, (*ii*) adsorption of the redox-active compound, (*iii*) electron transfer and possibly chemical reactions involving the adsorbed species, (*iv*) desorption of the product(s), and (*v*) diffusion of the product(s) to the bulk solution.[4, 6, 26, 57] The slowest step(s) in this sequence generally controls the overall reaction rate. For some redox-active minerals, the rate at which

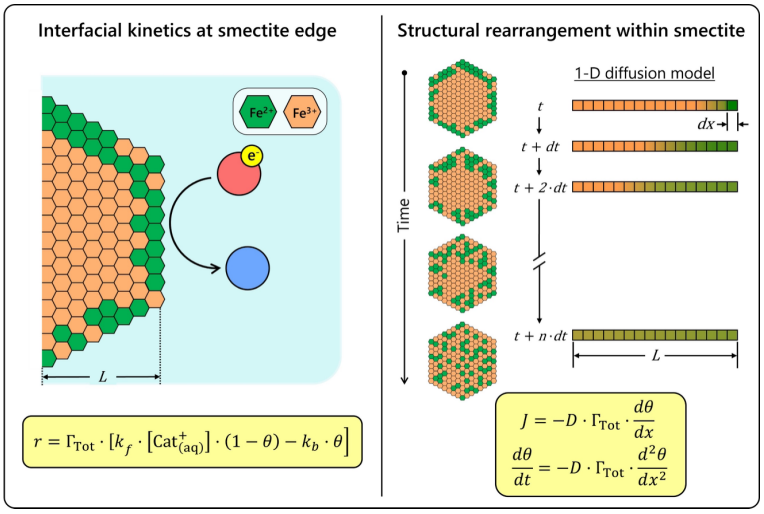

Figure 1. Schematic representation of the interfacial reaction occurring at the edge site of a smectite particle during a mediated reduction experiment and the generation of a chemical potential gradient between the surface and bulk due to differences in the $Fe^{2+}_{(s)}/Fe_{Total}$ ratio.

redox-active surface sites are regenerated can also be sufficiently slow to affect the overall reaction rate. This slow regeneration may occur if species must diffuse through the crystal lattice or if structural rearrangements are needed within the crystal structure to maintain local charge balances.[43, 50, 51] Here, we present a model framework to describe the kinetics of redox reactions at the edge site of a smectite particle when the aqueous diffusion and adsorption of the redox-active compound and its product(s) are sufficiently fast that the reaction rate is predominantly controlled by the electron transfer step(s) at the smectite-water interface and the rate at which redox-active surface sites are regenerated via diffusion within the solid. The following subsections describe the frameworks used to determine (*i*) the E_H value of Fe at or near the surface, (*ii*) the kinetics of electron transfer at the interface, and (*iii*) the rate at which the Fe sites are regenerated at the smectite surface for subsequent reactions.

Determining the E_H value of Fe at the smectite-water interface.

The reduction and oxidation of the Fe in smectites can be described using the simplistic half-reaction in **eq. 1**.[16, 18, 27] In this half-reaction, structural $Fe^{3+}_{(s)}$ is reversibly reduced to $Fe^{2+}_{(s)}$ by accepting an electron from an electron donor. The change in charge is compensated by the uptake of a monovalent cation, Cat^{+} (e.g., Li^{+}, Na^{+}, or K^{+}), or a proton into the interlayer.[16, 18, 27] Previous work found that charge compensation in the interlayer occurs primarily by the uptake of cations, not protons, at circumneutral pH values.[58, 59] For the data analyzed in the present study, we could not differentiate between cation and proton uptake because sodium uptake was not measured and a pH buffer was present in solution. Consequently, the model assumes that charge compensation occurs exclusively through cation (i.e., Na^{+}) uptake and release. This assumption does not influence the model output, as both the aqueous Na^{+} and H^{+} concentrations in the solution remained constant under the experimental conditions that were simulated.

Equilibrium reduction potential values of half reactions are typically determined using the Nernst equation, which is a function of the standard reduction potential (E^0_H) and the activities of the species.[60] The Nernst equation, however, is only applicable for sufficiently dilute solutions and pure solid phases.[31, 60, 61] In highly concentrated systems, including solid phases with compositions that vary as a function of redox state, interactions between charged species (e.g., $Fe^{2+}_{(s)}$, $Fe^{3+}_{(s)}$, and $Cat^{+}_{(s)}$) in close proximity to one another must be taken in account.[18, 61, 62] The Nernst-Frumkin isotherm, also referred to as Frumkin intercalation isotherm, accounts for these interactions when determining the equilibrium reduction potential ($E_{H,\theta,eq}$) of a solid:[31, 34, 53, 60-62]

$$E_{H,\theta,eq} = E^0_H - \frac{RT}{nF}\ln\left[\frac{\theta}{1-\theta}\right] + \frac{RT}{nF}\ln\{Cat^{+}_{(aq)}\} + \frac{RT}{F}g(0.5-\theta) \quad (2)$$

where E_{H}^{0} is the standard reduction potential (at $Fe^{2+}_{(s)}/Fe_{Total}$ = 0.5) of the smectite (assumed to be at pH 7.5 in this work because that is the pH value used to make previous measurements), R is the ideal gas constant (8.314 $J{\cdot}K^{-1}{\cdot}mol^{-1}$), T (K) is temperature, F is Faraday's constant (96,485 $C{\cdot}mol^{-1}$), and n is the number of electrons participating in the half reaction (n = 1 for **eq. 1**). The variable θ represents the $Fe^{2+}_{(s)}/Fe_{Total}$ ratio at the smectite surface, and $\{\mathrm{Cat}^{+}_{(\mathrm{aq})}\}$ is the activity of the monovalent cation in the electrolyte. The dimensionless interaction parameter, g, conventionally has been used to describe the interaction between adjacent reactive sites in an intercalation material, where $g < 0$ indicates favorable interactions, and $g > 0$ indicates unfavorable interactions.[34, 52] The g term reflects the impact of non-ideal charge interactions on the $E_{\mathrm{H},\theta,\mathrm{eq}}$ value (and ΔG_{rxn}) for the half-reaction in **eq. 1**, due to changes in the $Fe^{2+}_{(s)}/Fe_{Total}$ ratio at the smectite surface. Additionally, past studies have shown that Fe atoms in smectites occupy different coordination environments, leading to a distribution of reduction potentials for structural $Fe^{2+/3+}$ redox couple.[18, 21, 22] This distribution broadens the potential window over which the smectite remains redox active,[21, 22] and, the g term can be used to describe this behavior in the context of smectites.

Kinetics of interfacial electron transfer.

The electron transfer reaction between the redox-active compound and Fe atoms at the edge of the smectite particle is depicted in **Figure 1** and the rate of this reaction described by the following rate expression:

$$r = \Gamma_{\mathrm{Tot}} \cdot \left[k_f \cdot \left[\mathrm{Cat}^{+}_{(\mathrm{aq})}\right] \cdot (1-\theta) - k_b \cdot \theta\right] \quad (3)$$

where r (mol·cm^{-2}·s^{-1}) is a surface-normalized reaction rate, k_f (cm^4·mol^{-1}·s^{-1}) is the forward (reduction) reaction rate constant, k_b (cm·s^{-1}) is the backward (oxidation) reaction rate constant, and $\left[\mathrm{Cat}^+_{(aq)}\right]$ (mol·cm^{-3}) is the cation concentration in the electrolyte. The term Γ_{Tot} is the concentration of surface Fe sites (mol·cm^{-3}), and it is defined as:

$$\Gamma_{\mathrm{Tot}} = SSA \cdot SL \cdot site\ denisty \tag{4}$$

where *SSA* is the specific surface area of the smectite (cm^2·g^{-1}), *SL* is the solids loading of smectite in solution (g·cm^{-3}), and *site density* represents the surface density of reactive sites on the smectite surface (mol·cm^{-2}). Note that k_f and k_b have different units because their reaction orders differ. Both k_f and k_b are determined using the Butler-Volmer equation, which is conventionally used to describe electron transfer kinetics occurring at solid-liquid interfaces:[17, 18, 34, 52, 60]

$$k_f = \frac{k_0}{\left[\mathrm{Cat}^+_{(aq)}\right]_{\mathrm{ref}}} \cdot \exp\left((-\alpha) \cdot \frac{nF}{RT} \cdot (E_{\mathrm{H}} - E_{\mathrm{H},\theta})\right) \tag{5}$$

$$k_b = k_0 \cdot \exp\left((1-\alpha) \cdot \frac{nF}{RT} \cdot (E_{\mathrm{H}} - E_{\mathrm{H},\theta})\right) \tag{6}$$

where k_0 (cm·s^{-1}) is the standard heterogeneous rate constant for the reaction, $\left[\mathrm{Cat}^+_{(aq)}\right]_{\mathrm{ref}}$ is the standard reference concentration (1·10^{-3} mol·cm^{-3}), and α is a dimensionless electron transfer coefficient ($0 < \alpha < 1$), which represents the "closeness" of the reaction intermediate to either the reactant ($\alpha < 0.5$) or the product ($\alpha > 0.5$) in **eq. 1**.[60] The term '$E_{\mathrm{H}} - E_{\mathrm{H},\theta}$' in **eqs. 5** and **6** represent the electrochemical potential difference between the soluble redox-active compound in solution and the Fe redox couple on the smectite surface. The reduction potential of the redox-active compound is represented by E_{H} and the equilibrium potential of structural Fe at the smectite surface, $E_{\mathrm{H},\theta}$, is determined using:[44, 45]

$$E_{\mathrm{H},\theta} = E_{\mathrm{H}}^{0} + \frac{RT}{F} g(0.5 - \theta) \quad (7)$$

where **eq. 7** describes the variation in the surface potential of the structural Fe as a function of θ. Note that we use a singular standard heterogeneous rate constant, k_0, to describe both the forward and backward redox reaction in **eqs. 5** and **6**. This is based on the assumption that both reduction and oxidation occur along the same reaction coordinate and that the local environment of the Fe atom, where charge transfer occurs, remains spatially consistent.[60] Although this is a simplifying assumption and may not fully capture the kinetic variations caused by differences in the local coordination environment of Fe atoms in smectites, it still offers an adequate representation of the interfacial kinetics at the smectite-water interface.

The rate of structural rearrangement of charged species within the smectite lattice.

As structural Fe at the smectite surface is reduced or oxidized, the $Fe^{2+}{}_{(s)}/Fe_{Total}$ ratio at the surface begins to differ from the ratio deeper within the particle, creating a chemical potential gradient within the crystal lattice. To dissipate the chemical potential gradient, charged species rearrange themselves within the crystal lattice. In dioctahedral smectites (i.e., smectites with vacancies in the octahedral sheet), the rearrangement has been proposed to be controlled by rearrangement of Fe atoms and/or intervalence electron transfer reactions between adjacent Fe atoms in Fe^{2+}-O-Fe^{3+} linkages.[1, 18, 49, 51, 54, 63] In a previous study we demonstrated that the dissipation of the chemical potential gradient within an intercalation material can be successfully modeled using a one-dimensional diffusion model based on Fick's laws:[55]

$$J = -D \cdot \Gamma_{\mathrm{Tot}} \cdot \frac{d\theta}{dx} \quad (8)$$

$$\frac{d\theta}{dt} = -D \cdot \Gamma_{\mathrm{Tot}} \cdot \frac{d^2\theta}{dx^2} \tag{9}$$

where, J (mol·cm^{-2}·s^{-1}) represents the flux of charged species across a plane and D (cm^2·s^{-1}) represents the apparent diffusion coefficient of the redox sites in the clay matrix. Note that we use the term 'apparent' before the diffusion coefficient to indicate that the exact mechanism responsible for the dissipation of the chemical potential gradient remains uncertain. The parameter D represents a composite property that describes either the translocation of Fe atoms, electron hopping between adjacent Fe atoms, diffusion of cations through the smectite interlayers, or a combination of these processes.[1, 18, 49, 51, 54, 63] Additionally, D is assumed to be constant throughout the smectite particle and does not account for spatial heterogeneities that may exist within the particle. A schematic of the interfacial electron transfer reaction and the subsequent diffusion process, which dissipates the concentration gradient within the smectite particle, is provided in **Figure 1**.

In our model, the temporal step is represented by dt (1 second) and the spatial resolution of the finite-element, dx (cm), is calculated using the following equation:

$$dx = \sqrt{\frac{D \cdot dt}{D_M}} \tag{10}$$

where, D_M (0.45) is the dimensionless simulation constant and has a value less than 0.5 to maintain the numerical stability of the finite-element diffusion model, as explained in previous modeling studies.[60, 64, 65] The characteristic length, L, of the smectite clay particle is given by its radius, and is assumed to $2.5 \cdot 10^{-5}$ cm (0.25 microns) based on the size fraction used by Gorski et al. for the mediated electrochemical experiments.[14] The smectite particle is divided into N elements of thickness dx where $N = L/dx$. Note that in **eqs. 2, 3,** and **7**, the variable θ represents the

$Fe^{2+}_{(s)}/Fe_{Total}$ at the smectite surface, referring solely to the first element among N elements of the clay particle. Conversely, in **eq. 8** and **9**, θ represents the $Fe^{2+}_{(s)}/Fe_{Total}$ ratio in elements 2 through N.

Using the model to revisit the interpretation of mediated electrochemical measurements.

In the mediated electrochemical reduction and oxidation experiments conducted by Gorski et al.,[14, 21, 22] a constant potential was applied to a working electrode immersed in an electrolyte solution (i.e., 0.1 M $NaClO_4$ buffered at pH 7.5) containing a redox-active mediator. A small, known amount of smectite suspension was then added to the solution, and the current response was measured. For these experiments, we assumed that the redox-active compound was already in equilibrium with the working electrode when the smectite was added, and that the E_H value of the solution reflects the potential applied on the working electrode (i.e., the E_H values in **eq. 5** and **6** are known). The current response, i (A) produced when a known quantity of smectite was added to the solution can then be determined using the following equation:

$$i = n \cdot F \cdot A \cdot r \tag{11}$$

where, A (cm^2) is the active surface area of the smectite particles, n = 1, and r is represented by **eq. 3**. Note that this equation only holds true when the kinetics of electron transfer between the redox-active compound and the working electrode are significantly faster than the electron transfer between the redox-active compound and the smectite particle, which is assumed to be the case in this study.[56] At the end of the experiment, the simulated current-time curve is integrated to determine the net change in the bulk $Fe^{2+}_{(s)}$ (mol) concentration in the smectite particle using Faraday's law:

$$\Delta \mathrm{Fe}_{(s)}^{2+} = \frac{1}{nF} \int_{0}^{t_{\mathrm{cutoff}}} i \cdot dt \quad (12)$$

where t_{cutoff} is the cutoff time and is the time-step until which the simulated current-time curve is integrated. An example of how t_{cutoff} is implemented to the simulated current-time curve is illustrated in **Figure S4**. In the case of the mediated electrochemical experiments conducted by Gorski et al., the cutoff was approximately 30 minutes.[14, 21, 22] The final bulk $Fe^{2+}{}_{(s)}/Fe_{Total}$ ratio for the applied E_H is calculated using the following equation:

$$\mathrm{Fe}_{(s)}^{2+}/\mathrm{Fe}_{\mathrm{Total}} = \frac{\mathrm{Fe}_{(s),\mathrm{initial}}^{2+} + \Delta \mathrm{Fe}_{(s)}^{2+}}{\Gamma_{\mathrm{Tot}} \cdot A \cdot L} \quad (13)$$

where $\mathrm{Fe}_{(s),\mathrm{initial}}^{2+}$ (mol) is the initial number of $Fe^{2+}{}_{(s)}$ sites in the smectite particle before mediated electrochemical reduction or oxidation. The $Fe^{2+}{}_{(s)}/Fe_{Total}$ ratio is then plotted as a function of applied E_H to generate the redox profile.

RESULTS AND DISCUSSION

Simulating mediated electrochemical reduction and oxidation of Fe in SWa-1.

To validate the model's capability of reproducing experimentally collected data, we initially simulated the mediated electrochemical reduction and oxidation experiments with ferruginous smectite, SWa-1 (**Figure 2**).[21] To generate the *reduction* curves (red-dashed line, **Figure 2**), we simulated the electrochemical reduction of fully re-oxidized SWa-1 clay (i.e., initial bulk $Fe^{2+}{}_{(s)}/Fe_{Total}$ ratio = 0.01) at different E_H values ranging from +0.65 to -0.65 V vs. SHE at 0.01 V intervals. Note that we simulated re-oxidized SWa-1, as opposed to native SWa-1, because the dithionite reduction process is known to irreversibly alter the structural and chemical properties

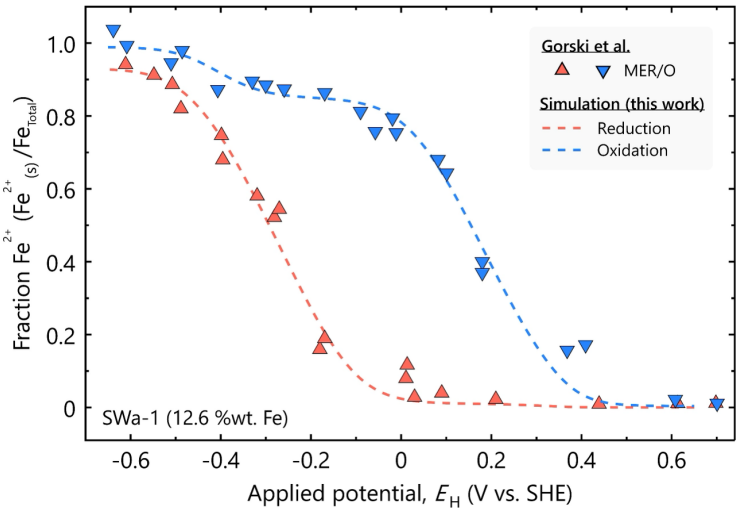

Figure 2. Simulated redox profiles of SWa-1 fitted to experimental redox profiles collected by Gorski et al.[21,22] The Gorski et al. data includes the re-oxidized, re-re-oxidized, reduced, and re-reduced datasets. The parameters used to achieve the fit for SWa-1 were E_H^0 = – 0.01 V vs. SHE, k_0 = 2.5·10^{-10} cm·s^{-1}, D = 7.5·10^{-13} cm^2·s^{-1}, α = 0.52, and g = 9. A t_{cutoff} value of 30 minutes was assumed for generating the *reduction* (red-dashed line) and *oxidation* (blue-dashed line) profiles. Initial $Fe^{2+}_{(s)}/Fe_{Total}$ values of 0.01 and 0.85 were used for simulating the *oxidation* and *reduction* curves, respectively.

of smectite.[13, 14, 21, 22, 49] Thus, the native and reduced SWa-1 were most likely structurally different, whereas the re-oxidized and reduced SWa-1 were likely structurally more similar. To mimic the experiments performed by Gorski et al., the simulation cutoff time was set to 30 minutes.[21, 22] This meant that only the first 30 minutes of the simulated current response was considered when calculating the change in the $Fe^{2+}_{(s)}/Fe_{Total}$ ratio at an applied E_H. The simulated $Fe^{2+}_{(s)}/Fe_{Total}$ ratios were plotted against E_H to generate the reduction profile. The *oxidation* curve (blue-dashed line, **Figure 2**) was generated in a similar fashion to the reduction profile, with the only difference being that the re-oxidized SWa-1 was assumed to be fully reduced (i.e., initial bulk $Fe^{2+}_{(s)}/Fe_{Total}$ ratio = 0.99) before being electrochemically oxidized. The simulated redox curves were fitted to the experimental ones by floating multiple parameters and minimizing the least-squared differences between the two sets of curves over iterative cycles.[21, 22] The parameters that were

floated were the standard reduction potential (E_H^0), the standard heterogeneous rate constant (k_0), the apparent diffusion coefficient (D), the electron transfer coefficient (α), and the interaction parameter (g). Subsequently, we manually fine-tuned the fitted parameters to improve the overall fit quality.

The simulated data for the *reduction* of re-oxidized SWa-1 closely matched the experimental data collected by Gorski et al (**Figure 2**).[21, 22] However, the simulated data for the *oxidation* of reduced SWa-1 initially did not fully capture the data collected from the oxidation experiments (**Figure S5**). Specifically, the experimental and simulation data between E_H = – 0.4 V to 0.0 V differed, with the simulation calculating larger $Fe^{2+}_{(s)}/Fe_{Total}$ ratios than those experimentally recorded (refer to **Figure S5)**. When we changed the initial $Fe^{2+}_{(s)}/Fe_{Total}$ ratio in the reduced SWa-1 from 0.99 to 0.85 (i.e., only 85% of the Fe sites were reduced to $Fe^{2+}_{(s)}$ initially) for the oxidation simulations, the simulated and experimental curves converged (**Figure 2**).[21, 22] We speculate that the reduced SWa-1 used to generate the experimental data was incompletely reduced, which may have been caused by incomplete reduction by dithionite or inadvertant partial oxidation during subsequent storage.[21, 22] With this modification, the simulation successfully replicated the experimental redox curves collected for SWa-1 (**Figure 2**, r^2 = 0.98, n = 40).[21, 22] Importantly, the simulation described both the *reduction* and *oxidation* redox curves using the same parameters: E_H^0 (– 0.01 V vs. SHE) , k_0 ($2.5 \cdot 10^{-10}$ cm·s^{-1}), D ($7.5 \cdot 10^{-13}$ cm^2·s^{-1}), α (0.52), and g (9), meaning that the hysteresis could be due to the experimental cutoff time.

Sensitivity analyses of the simulations were performed to assess the uncertainty associated with each of the fitted redox parameters (**Section S3**). Based on the analyses, the

quality of fit between the simulated and experimental data was highly sensitive to changes in the E_H^0 value, exhibiting a narrow range of uncertainty in the predicted E_H^0 with values ranging from –0.11 V to +0.01 V vs. SHE. Relatively, k_0 displayed more uncertainty in its predicted value with the best fits occurring for k_0 values ranging between $2.0 \cdot 10^{-11}$ to $2.5 \cdot 10^{-9}$ cm·s^{-1}. Determining the uncertainty associated with D proved to be challenging as the quality of fit between the experimental and simulated data remained relatively constant for D values greater than 10^{-12} cm^2·s^{-1} (**Section S3**). However, the quality of fit deteriorated significantly for D values less than $5 \cdot 10^{-13}$ cm^2·s^{-1}, suggesting that the apparent diffusion of charge carriers in the smectite particle is likely higher than $5 \cdot 10^{-13}$ cm^2·s^{-1}. The uncertainty in α ranged between 0.3 and 0.7, and the quality of fit was insensitive to changes in g for values ranging between 0 and 30. Collectively, the sensitivity analyses indicated that E_H^0 and k_0 influenced the simulated redox profile of SWa-1 the most. Although D did not significantly affect the fit quality for values above 10^{-12} cm^2·s^{-1} (**Section S3**), it was essential for capturing the trend in the experimental data between E_H = – 0.6 V to – 0.5 V, where the $Fe^{2+}_{(s)}/Fe_{Total}$ ratio value plateaus but does not reach 1 in the *reduction* experiment (**Figure 2**). The relatively low sensitivity of α and g on the quality of the fit can be attributed to the narrower range of values used for these parameters during the fitting process, compared to the wider range used for k_0 and D, which differed by orders of magnitude. Examples depicting the effect of each parameter on the simulated redox curves are provided in **Figure S7**.

Effect of equilibration time on redox hysteresis.

After validating the accuracy of our simulations with the experimental redox curves of SWa-1 (**Figure 2**),[21, 22] we proceeded to test our hypothesis that redox hysteresis was due to insufficient

equilibration time in the mediated electrochemical experiments using two approaches. First, we simulated *reduction* and *oxidation* experiments of SWa-1, varying the cutoff time to determine if the extent of redox hysteresis decreased with increasing cutoff time. In these simulations, the cutoff time represented the duration allowed for the clay particles to be reduced or oxidized by a redox mediator under a constant applied E_H. Second, we performed experiments in which we allowed reduced SWa-1 to equilibrate with an electron mediator for a longer period (12-24 hours) and measured E_H for samples having different $Fe^{2+}_{(s)}/Fe_{Total}$ ratios.

The *reduction* and *oxidation* curves at varying cutoff times were simulated using the best-fit parameters used to simulate the redox curve of SWa-1 in **Figure 2**, which had a cutoff time of

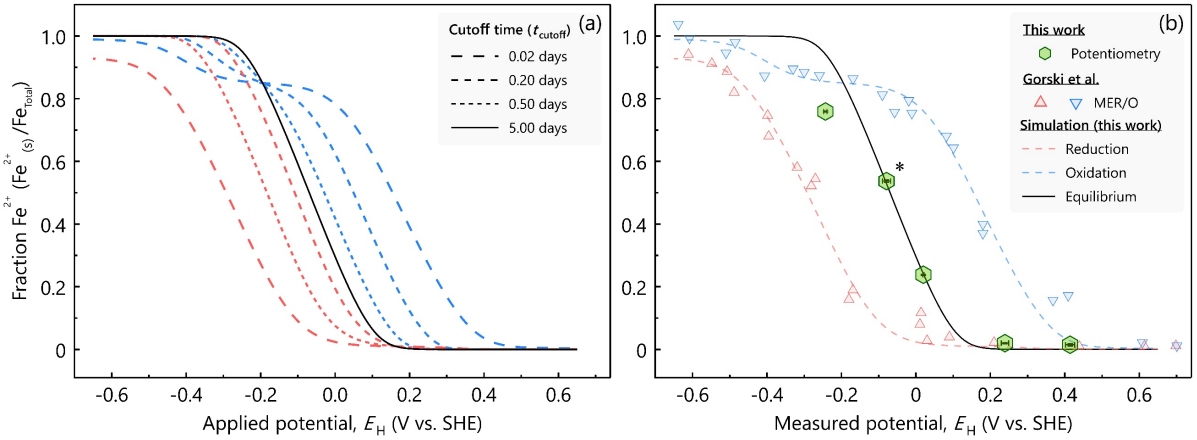

Figure 3. (a) Effect of cutoff time (t_{cutoff}) on the redox profiles generated from the simulated *reduction* and *oxidation* experiments on SWa-1, and **(b)** mediated potentiometry measurements of reduced and re-oxidized SWa-1 (green hexagonal marker); the data points from the mediated electrochemical experiments performed by Gorski et al. and the redox profiles from the simulations are included as reference to help guide the reader.[21, 22] The green hexagonal data points represent the average of triplicate mediated potentiometry measurements, and the error bars indicate the standard deviation. Note that '∗' denotes the SWa-1 sample treated with 30 µL of 1.0 M hydrogen peroxide which had leaked in transit to Mössbauer analysis leading to an underestimated Fe^{2+}/Fe_{Total} ratio of 0.11 (**Section S2**). A corrected Fe^{2+}/Fe_{Total} ratio of 0.53 was used when plotting the data point against the corresponding E_H. Details on how the Fe^{2+}/Fe_{Total} ratio was calculated are provided in **Section S5** of the supplemental text.

30 minutes. The extent of redox hysteresis in the simulations of the *reduction* and *oxidation* experiments decreased as the cutoff time employed in the simulation was increased from 0.02 days to 5.00 days as seen in **Figure 3**, panel a. The separation between the redox curves generated from the simulated *reduction* and *oxidation* experiments gradually approached each other as the cutoff time increased. At a cutoff time of approximately 4.75 days, both redox curves converged to form a single redox curve represented by the solid black line in **Figure 3**a**,** indicating that the SWa-1 particles had reached equilibrium in the simulation. Further increasing in the cutoff time (e.g., $t_{\text{cutoff}} > 4.75$ days) did not affect the simulated redox curves. Notably, the 'equilibrated' redox curve (solid black line in **Figure 3**, panel a) could fully be described by the Nernst-Frumkin equation (**eq. 2**) without the need for any kinetic or diffusion terms. This mathematical consistency arises because the rate equation (**eq. 3**) reduces to the Nernst-Frumkin equation when equilibrium conditions are assumed (refer to **Section S4** in SI for derivation). At equilibrium, the equilibrated redox curve for SWa-1 exhibited an $Fe^{2+}{}_{(s)}/Fe_{Total}$ ratio of 0.50 at an E_H value of – 0.07 V vs. SHE, which was 60 mV more negative than that of the fitted value of E_H^0 = – 0.01 V vs SHE. This shift is attributed to the dependence of the reduction potential on the activity of Na^+, which was assumed to be 0.1 in the simulation due to the use of 0.1 M $NaClO_4$ in the experiments.[21, 22] Note that the time required to reach equilibrium depends on both k_0 and D, and is influenced by the active surface area and size of the clay particles in suspension. We speculate that smaller particles may equilibrate faster if charge transfer occurs predominantly at edge sites, due to the shorter distance between the edge and center, and their relatively larger active surface area.

An interesting observation from the simulations with varying cutoff times was that all simulated *oxidation* curves in **Figure 3**a consistently intersected the equilibrated redox curve at an

E_H value of – 0.195 V vs. SHE and an $Fe^{2+}_{(s)}/Fe_{Total}$ ratio of 0.85, whereas the simulated *reduction* curves never intersected the equilibrated redox curve. This crossover of the *oxidation* curves with the equilibrated redox curve arises from the assumption that the initial $Fe^{2+}_{(s)}/Fe_{Total}$ ratio in SWa-1 was 0.85 (i.e., not fully reduced). Based on the equilibrated redox curve (black line in **Figure 3**, panel a) and **eq.2**, an SWa-1 sample with an $Fe^{2+}_{(s)}/Fe_{Total}$ ratio of 0.85 would have a reduction potential of – 0.195 V vs. SHE. This implies that at E_H values more positive than – 0.195 V, the SWa-1 would undergo oxidation, while at E_H values more negative than – 0.195 V, the SWa-1 would undergo reduction. This behavior is reflected in the simulated *oxidation* curves in **Figure 3**a, where data points to the right of the equilibrated redox curve (i.e., E_H > – 0.195 V vs. SHE) represent oxidation, while data points to the left (i.e., E_H < – 0.195 V vs. SHE) actually represent reduction. This effect is more evident when comparing the 30-minute *oxidation* curves depicted in **Figure S4**, where the *oxidation* curves were simulated with initial $Fe^{2+}_{(s)}/Fe_{Total}$ ratios of 0.85 and 0.99. The *oxidation* curve simulated using an initial $Fe^{2+}_{(s)}/Fe_{Total}$ ratio of 0.99 does not cross over the equilibrated redox curve, as all points represent oxidation (compare blue dashed lines in **Figure 3**a and **Figure S4**). Note that, despite the *oxidation* curve not necessarily representing oxidation at all E_H values, within this study, we continue to use the term '*oxidation*' for brevity when referring to the curves fitted to the data obtained from the mediated electrochemical oxidation experiments.[21, 22]

After studying the impact of cutoff time on the simulated redox curves of SWa-1, we proceeded to experimentally validate our observations from the simulation. We hypothesized that the E_H values of the SWa-1 samples measured during mediated potentiometry experiments would lie in between the SWa-1 redox curves collected by Gorski et al. due to the longer

equilibration time provided in our experiments (12-24 hours compared to 30 minutes).[21, 22] Based on this hypothesis, we performed mediated potentiometric measurements on SWa-1 samples with varying $Fe^{2+}_{(s)}/Fe_{Total}$ ratios (**Figure 3**, panel b).

These samples were prepared by reducing SWa-1 with sodium dithionite, then reoxidizing samples to various extents by adding different amounts of 1.0 M hydrogen peroxide (experimental details in **Section S1**) and allowing the reaction to proceed for at least 24 hours. The extent of reduction and reoxidation (i.e., $Fe^{2+}_{(s)}/Fe_{Total}$ ratio of each sample) of the chemically treated SWa-1 samples were determined using ^{57}Fe Mössbauer spectroscopy analysis (experimental details and Mössbauer spectra of each sample are provided in **Section S2**). The E_H values of the SWa-1 samples with differing $Fe^{2+}_{(s)}/Fe_{Total}$ ratios were measured using mediated potentiometry (experimental details are provided in **Section S6**). Note that SWa-1 suspensions were allowed to equilibrate with the mediator in the electrolyte for 12-24 hours before the E_H measurements were recorded. The measured E_H values at pH 7.0 were normalized to pH 7.5 by subtracting 30 mV (i.e., 59 mV per pH decade multiplied by 0.5 pH units) from the measured value to ensure consistency between the E_H values and the SWa-1 data collected by Gorski et al.[18, 56]

The measured E_H values of the SWa-1 samples closely matched the equilibrated redox curve of SWa-1 (**Figure 3**, panel b**,** r^2 = 0.98, n = 5), supporting our hypothesis that extended equilibration times mitigate redox hysteresis. Note that the data collected by Gorski et al. used mediated electrochemical reduction/oxidation, which is fundamentally different from the mediated potentiometry used in this study.[14, 21, 22] Mediated electrochemical reduction/oxidation

436 is an active technique that measures the change in the $Fe^{2+}_{(s)}/Fe_{Total}$ ratio by integrating the current
437 response observed when an aliquot of oxidized or reduced clay mineral is added to a pH-buffered
438 electrolyte containing a mediator maintained at a fixed E_H value.[22, 56] This approach has an
439 inherent time limitation, as the current response can only be analyzed for a short period of time
440 before it decreases to the point where it becomes indistinguishable from the background
441 current.[22, 56] In contrast, mediated potentiometry is a passive technique where no current flows
442 through the system, and the clay mineral allowed to equilibrate with the mediator for durations
443 exceeding 12 hours.[25, 26] An important consequence of the two different approaches is that, in
444 mediated electrochemical reduction/oxidation, a gradient of $Fe^{2+}_{(s)}/Fe_{Total}$ develops during the
445 redox process, which must dissipate over time. However, in mediated potentiometry, where the
446 E_H values of clay minerals with different $Fe^{2+}_{(s)}/Fe_{Total}$ ratios are measured, no such gradient exists,
447 as the bulk of the clay mineral is already in an equilibrated state. We fit the data points obtained
448 from mediated potentiometry in this study to the Nernst-Frumkin equation (**eq. 2**) to test whether
449 the fitted E_H^0 value deviated significantly from the E_H^0 value obtained from the fits of the *reduction*
450 and *oxidation* curves. The fit produced and E_H^0 value of – 0.017 V vs. SHE (r^2 = 0.92, n = 5), which
451 was remarkably close to the E_H^0 value (– 0.01 V vs. SHE) determined by fitting the *reduction* and
452 *oxidation* curves.

453 **Simulating the redox curves of NAu-1, NAu-2, and SWy-2.**

454 After confirming that our simulations accurately replicated the data from the mediated
455 electrochemical experiments conducted on SWa-1 (**Figure 2**) and demonstrating that the redox
456 hysteresis was likely due to insufficient equilibration time for the smectite particles (**Figure 3**), we

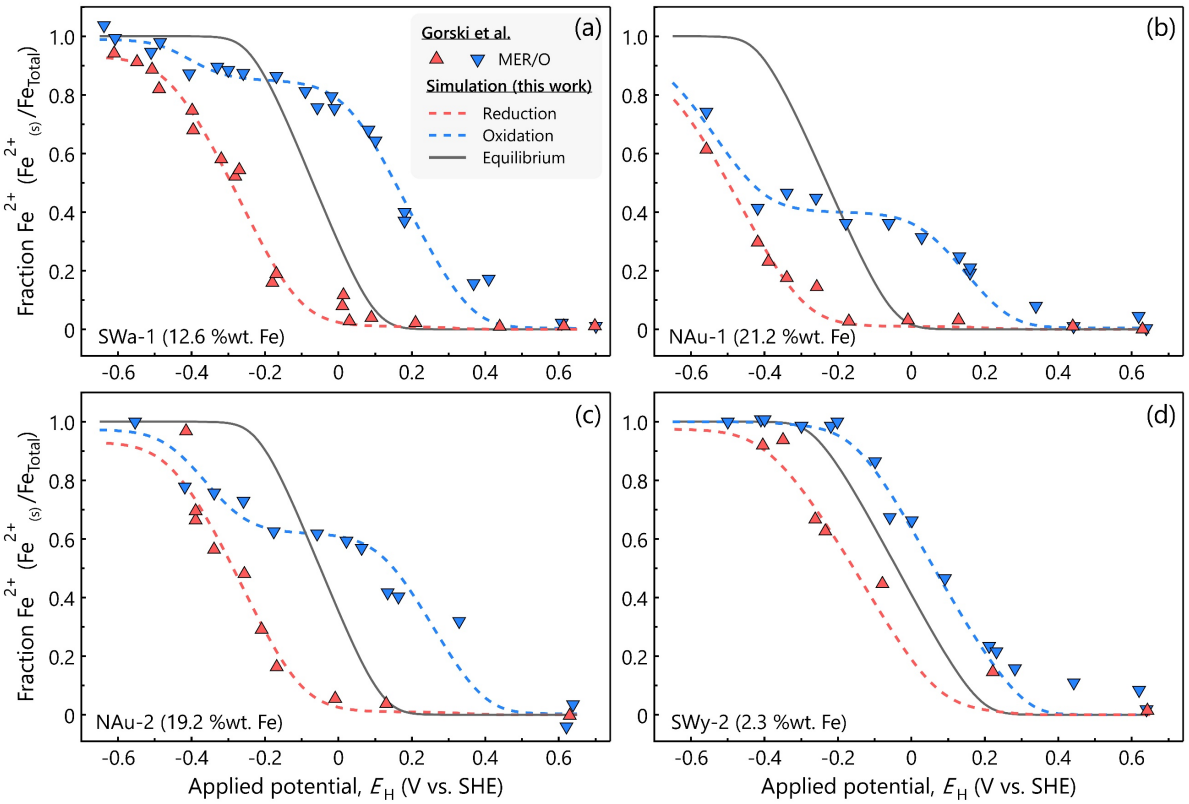

Figure 4. Simulated redox profiles of four smectites – **(a)** SWa-1, **(b)** NAu-1, **(c)** NAu-2 and **(d)** SWy-2 – fitted to experimental redox profiles collected by Gorski et al.[21,22] The parameters used to achieve the fit are provided in **Table 1**. The *reduction* and *oxidation* experiment simulations are represented by the dashed red and blue lines, respectively. The solid black line represents the equilibrated redox curve. All simulation fits had an r^2 value greater than 0.94. The initial $Fe^{2+}_{(s)}/Fe_{Total}$ ratio used for simulating the *oxidation* curves are 0.85 (SWa-1), 0.40 (NAu-1), 0.62 (NAu-2), and 0.99 (SWy-2).

457 expanded our simulations to include the *reduction* and *oxidation* experiments conducted by Gorski
458 et al. on three other smectites: nontronite NAu-1 (21.2 % wt. Fe), nontronite NAu-2 (19.2 % wt.
459 Fe), and Wyoming montmorillonite SWy-2 (2.3 % wt. Fe). The simulated redox and experimental
460 data for the *reduction* and *oxidation* experiments conducted on all four clays are shown in **Figure**
461 **4**, and the simulation parameters used to achieve the fit for the four clays are provided in **Table**
462 **1**.[22] The simulated redox curves of the *reduction* experiments closely matched the experimental
463 data collected by Gorski et al. for all four smectites (compare red dashed lines with red upward

Table 1. Model parameters used to simulate the redox curves of smectites SWa-1, NAu-1, NAu-2, and SWy-2.

Smectite	E_H^0 (V vs. SHE)	k_0 (cm·s^{-1})	D (cm^2·s^{-1})	t_{eqb}[a] (days)	α	g	r^2
SWa-1	– 0.01	$2.5 \cdot 10^{-10}$	$7.5 \cdot 10^{-13}$	4.75	0.52	9	0.98
NAu-1	– 0.17	$1.0 \cdot 10^{-10}$	$6.2 \cdot 10^{-13}$	7.63	0.52	10	0.97
NAu-2	+ 0.01	$1.9 \cdot 10^{-10}$	$7.7 \cdot 10^{-13}$	5.32	0.52	10	0.94
SWy-2	+ 0.02	$2.0 \cdot 10^{-9}$	$1.2 \cdot 10^{-12}$	0.52	0.48	13	0.98

[a]The cutoff time taken to reach equilibrium in a mediated electrochemical reduction/oxidation is represented by t_{eqb} and r^2 represents the quality of fit between the simulated and experimental data in **Figure 3**. The uncertainty associated with the extracted model parameters are provided in **Section S3** of the SI.

facing triangles in **Figure 4**) without any modifications to the initial $Fe^{2+}_{(s)}/Fe_{Total}$ ratio of 0.01.[22] However, as with SWa-1, fitting the redox curves for the *oxidation* experiments required us to adjust the initial $Fe^{2+}_{(s)}/Fe_{Total}$ ratio to a value lower than 0.99 for NAu-1 and NAu-2 to ensure convergence between the experimental and simulated data (compare blue dashed lines with blue downward facing triangles in **Figure 4**, panels a-c**)**. An initial $Fe^{2+}_{(s)}/Fe_{Total}$ ratio of 0.40 (NAu-1) and 0.62 (NAu-2) was used to achieve convergence (**Figure 4**, panels b and c). Note that the initial $Fe^{2+}_{(s)}/Fe_{Total}$ ratio of 0.40 (i.e., 40% of the total Fe was reduced to $Fe^{2+}_{(s)}$) for NAu-1 is close to the experimentally determined value of 0.45 from the original study based on Mössbauer analysis.[22] Unlike the iron-rich smectites, we were able to simulate the redox profile for the *oxidation* experiments conducted on SWy-2 without any change to the initial $Fe^{2+}_{(s)}/Fe_{Total}$ ratio of 0.99, suggesting that SWy-2 was completely reduced before being electrochemically oxidized (**Figure 4**, panel d). Overall, the simulations accurately replicated the experimental redox curves collected by Gorski et al. for NAu-1 (**Figure 4**, panel b, $r^2 = 0.97$, $n = 23$), NAu-2 (**Figure 4**, panel c, $r^2 = 0.94$, $n = 23$), and SWy-2 (**Figure 4**, panel d, $r^2 = 0.99$, $n = 23$).[22]

Extended *reduction* and *oxidation* experiment simulations were also conducted on the three other clays to determine their equilibrated redox curves. The equilibrated redox profile for each clay is represented by the solid black lines in **Figure 4**. The cutoff time required to reach equilibrium differed among the four smectites. SWy-2 equilibrated the fastest with a cutoff time of 0.52 days and NAu-1 equilibrated the slowest with a cutoff time of 7.63 days; NAu-2 equilibrated with a cutoff time of 5.32 days. Interestingly, the cutoff time required to reach equilibrium bore a strong positive correlation against the % wt. Fe content of the smectite (r^2 = 0.93, n = 4), suggesting that smectites with higher Fe content would take longer to reach equilibrium.

Interpreting the redox properties of the smectites.

Based on our simulations, the E_{H}^{0} values at pH 7.5 for the four smectites were: – 0.17 (NAu-1), – 0.01 (SWa-1), + 0.01 (NAu-2) and + 0.02 (SWy-2) V vs. SHE (**Table 1**). The range of values defining the uncertainty in the fitted E_{H}^{0}, k_0 and D values are provided in **Table S3**. The trend observed in the fitted E_{H}^{0} values aligned with the apparent standard reduction potentials reported by Gorski et al. for native smectites, where SWy-2 exhibited the highest apparent standard reduction potential ($E_{\mathrm{H}}^{\emptyset}$ = – 0.03 V vs. SHE) and NAu-1 the lowest ($E_{\mathrm{H}}^{\emptyset}$ = – 0.45 V vs. SHE).[22] However, the E_{H}^{0} values spanned a narrower range (0.19 V) than the $E_{\mathrm{H}}^{\emptyset}$ values reported by Gorski et al. (0.42 V), suggesting that the affinity of structural Fe to gain or lose electrons did not vary among the four smectites as our original interpretation indicated.[22] Prior studies have shown that the reactivity of the dioctahedral Fe in smectites is influenced by its coordination environment, where an Fe^{2+} atom adjacent to a Mg^{2+} or another Fe^{2+} atom was oxidized prior to an Fe^{2+} atom associated

499 with an Al^{3+} atom.[18, 66] We speculate that the E_H^0 value of a smectite is dependent on the relative
500 abundance of Mg^{2+}-O-$Fe^{2+/3+}$, Fe^{3+}-O-$Fe^{2+/3+}$ and Al^{3+}-O- $Fe^{2+/3+}$ linkages in the smectite. Note that the
501 E_H^0 values reported in this study specifically apply to smectites that were chemically treated with
502 dithionite. Based on trends observed by Gorski et al. when comparing the $E_H^{\emptyset}$ values of unaltered
503 and dithionite-treated smectites,[22] we speculate that the E_H^0 for unaltered smectites would likely
504 be slightly more negative than those reported here.

505 Among the smectites investigated, SWy-2 exhibited the fastest kinetics with a standard
506 heterogeneous rate of $2.0 \cdot 10^{-9}$ cm·s^{-1} (**Table 1**). The standard heterogeneous rate constants for the
507 iron rich smectites were over an order of magnitude lower than SWy-2 with values ranging
508 between $1.0 \cdot 10^{-10}$ cm·s^{-1} (NAu-1) and $2.5 \cdot 10^{-10}$ cm·s^{-1} (SWa-1). Interestingly, the standard
509 heterogenous rate constants correlated strongly against the inverse of % wt. Fe in each smectite
510 ($r^2 = 0.99$, $n = 4$; **Figure S9**) suggesting that the heterogeneous rate constant captured some of the
511 structural aspects of the smectites investigated in this study. However, deducing conclusive
512 inferences based on this correlation would require a quantitative investigation of parameters such
513 as active surface area, particle size distribution, and exact masses of smectite added during the
514 mediated electrochemical experiments. The apparent diffusion coefficients of all four smectites
515 were similar, ranging from $6.2 \cdot 10^{-13}$ $cm^2 \cdot s^{-1}$ for NAu-1 to $1.2 \cdot 10^{-12}$ $cm^2 \cdot s^{-1}$ for SWy-2 (**Table 1**). While
516 these values were several orders of magnitude greater than reported proton diffusion values in
517 montmorillonite (10^{-19} $cm^2 \cdot s^{-1}$) and kaolinite (10^{-21} $cm^2 \cdot s^{-1}$),[67-69] they are only an order of magnitude
518 lower than the electron diffusion coefficient (10^{-11} $cm^2 \cdot s^{-1}$) reported by Rosso et al. for a defect free
519 iron rich smectites.[69, 70] The closeness of the reported electron diffusion coefficient and the
520 diffusion coefficients from this study (**Table 1**) suggests that electron migration in Fe^{2+}-O-Fe^{3+}

linkages may be the major process responsible for dissipating the chemical potential gradient within the iron rich smectites.[69, 70] The parameters α and g did not vary significantly among the four smectites. The α values for the four smectites ranged between 0.48 and 0.52 and g values ranged between 9 and 13 (**Table 1**).

ENVIRONMENTAL IMPLICATIONS

This work demonstrates that mediated electrochemical techniques have inherent limitations due to their short measurement times, which can potentially complicate data interpretation. Therefore, it is important to consider the processes that could limit the rate of the redox reaction being investigated. In this study, we found that when interpreting the mediated electrochemical reduction/oxidation data of smectites, both the electron transfer kinetics at the smectite-water interface and the internal charge reorganization within the smectite particle need to be considered. Furthermore, the Nernst-Frumkin isotherm fully captured the redox properties of the clay minerals under equilibrium conditions. The time required to reach equilibrium under oxidizing or reducing conditions varied across smectites, ranging from 0.52 days for SWy-2 to 7.63 days for NAu-1. This variation could have significant implications for how smectites behave in the environment when exposed to events that induce oxidizing or reducing conditions. These processes are particularly relevant in the context of 'biogeochemical batteries,' where the redox cycling of minerals like smectites plays a crucial role in the storage and transfer of electrons across environmental interfaces.[71] Depending on the duration of such events, the rate of smectite oxidation or reduction may be governed by the kinetics of charge transfer at the mineral surface or by the internal reorganization of charge within the mineral.[71] For instance, in the case of SWy-

2, redox events lasting for a day could result in full equilibration with its environment, whereas iron-rich smectites such as SWa-1, NAu-1, and NAu-2 may require significantly more time to reach equilibrium. Additionally, both processes should be considered when interpreting kinetic data from contaminant transformation studies, as the reaction rates observed in these studies can be influenced by either the interfacial electron transfer kinetics or the dissipation of the chemical potential gradient within the smectite particle.[4, 6, 7, 49] The process limiting the reaction rate depends on the thermodynamic driving force, represented by the difference in reduction potential between the contaminant and the smectite particle.[4, 6, 7, 49] The model developed here describes the reactivity of the smectite as a function of electrochemical potential difference (ΔE_{H}) between the smectite surface and the soluble redox compound (e.g., redox mediator and soluble organic matter that can act as electron donors/acceptors). One can potentially apply the model to describe the redox activity of minerals in systems where ΔE_{H} changes as function of time due to periodic oscillations in environmental conditions, such as changes in dissolved oxygen and chemical composition of groundwater caused by seasonal fluctuations in the groundwater table.[71-73]

The findings from this work may also offer an alternative hypothesis as to why biologically and chemically reduced smectites often exhibit different structural properties, even when samples are reduced to the same extents.[74] Prior work has largely speculated that the differences are due to bacteria preferentially reducing Fe^{3+} at edge sites, while chemical reductants react with both edge and basal Fe^{3+} sites.[74] We speculate that the structural differences could also be caused by the differences in the chemical driving force of reduction (ΔE_{H}) and the timescale over which reduction occurs. Microbial reduction involves a small driving force but long

equilibration time, often extending several days to weeks, [5, 11] while chemical reduction involves a large driving force and relatively short equilibration time. The $Fe^{2+}_{(s)}/Fe^{3+}_{(s)}$ gradient created during chemical reduction, but not biological reduction, may alter what types of structural modifications occur over the course of the reaction. While the model performs adequately in describing the redox properties of smectites in controlled environments, such as in the mediated electrochemical experiments conducted by Gorski et al.,[21, 22] it does not account for the presence of other cations, anions, or natural organic matter, which could alter the observed experimental trends. These species are expected to influence the aggregation behavior and interlayer spacing of clay minerals. Further experiments investigating the effect of these parameters on the redox properties of smectites would be necessary to accurately predict their behavior in more complex environmental conditions.

ASSOCIATED CONTENT

Supporting Information

The re-oxidation process of the smectite, E_H^0 values of the redox mediators used in this study, derivation of Nernst-Frumkin isotherm from rate equation, calaculation of $Fe^{2+}_{(s)}/Fe_{Total}$ ratio of leaked sample, and the mediated open-circuit potential profiles are provided in the supplemental text.

Supporting information (PDF)

AUTHOR INFROMATION

Corresponding Author

*E-mail: gorski@psu.edu; Phone: +1 814-865-5673

Notes

The authors declare no competing financial interests.

ACKNOWLEDGEMENTS

We thank Nehru Sambasiva Mantripragada (The University of Georgia, Athens) for performing Mössbauer analysis on the reduced and partially re-oxidized SWa-1 clay samples. This study was financially supported by the National Science Foundation (CBET – 1749207) and the Marcus Engineering Research Fellowship (The Pennsylvania State University). The opinions, findings, and conclusions expressed in this study are those of the authors and do not necessarily reflect the views of the funding sources.

REFERENCES

1. Komadel, P.; Lear, P. R.; Stucki, J. W., Reduction and reoxidation of nontronite: Extent of reduction and reaction rates. *Clays and Clay Minerals* **1990,** *38*, 203-208.
2. Hofstetter, T. B.; Schwarzenbach, R. P.; Haderlein, S. B., Reactivity of Fe (II) species associated with clay minerals. *Environmental science & technology* **2003,** *37*, (3), 519-528.
3. Elsner, M.; Schwarzenbach, R. P.; Haderlein, S. B., Reactivity of Fe (II)-bearing minerals toward reductive transformation of organic contaminants. *Environmental science & technology* **2004,** *38*, (3), 799-807.
4. Hofstetter, T. B.; Neumann, A.; Schwarzenbach, R. P., Reduction of nitroaromatic compounds by Fe(II) species associated with iron-rich smectites. *Environ Sci Technol* **2006,** *40*, (1), 235-42.
5. Kukkadapu, R. K.; Zachara, J. M.; Fredrickson, J. K.; McKinley, J. P.; Kennedy, D. W.; Smith, S. C.; Dong, H., Reductive biotransformation of Fe in shale–limestone saprolite containing Fe (III) oxides and Fe (II)/Fe (III) phyllosilicates. *Geochimica et Cosmochimica Acta* **2006,** *70*, (14), 3662-3676.
6. Neumann, A.; Hofstetter, T. B.; Lüssi, M.; Cirpka, O. A.; Petit, S.; Schwarzenbach, R. P., Assessing the redox reactivity of structural iron in smectites using nitroaromatic compounds as kinetic probes. *Environmental science & technology* **2008,** *42*, (22), 8381-8387.
7. Neumann, A.; Hofstetter, T. B.; Skarpeli-Liati, M.; Schwarzenbach, R. P., Reduction of polychlorinated ethanes and carbon tetrachloride by structural Fe (II) in smectites. *Environmental science & technology* **2009,** *43*, (11), 4082-4089.

8. Dong, H.; Jaisi, D. P.; Kim, J.; Zhang, G., Microbe-clay mineral interactions. *American Mineralogist* **2009,** *94*, (11-12), 1505-1519.
9. Bishop, M. E.; Dong, H.; Kukkadapu, R. K.; Liu, C.; Edelmann, R. E., Bioreduction of Fe-bearing clay minerals and their reactivity toward pertechnetate (Tc-99). *Geochimica et Cosmochimica Acta* **2011,** *75*, (18), 5229-5246.
10. Yang, J.; Kukkadapu, R. K.; Dong, H.; Shelobolina, E. S.; Zhang, J.; Kim, J., Effects of redox cycling of iron in nontronite on reduction of technetium. *Chemical Geology* **2012,** *291*, 206-216.
11. Luan, F.; Liu, Y.; Griffin, A. M.; Gorski, C. A.; Burgos, W. D., Iron (III)-bearing clay minerals enhance bioreduction of nitrobenzene by Shewanella putrefaciens CN32. *Environmental science & technology* **2015,** *49*, (3), 1418-1426.
12. Tsarev, S.; Waite, T. D.; Collins, R. N., Uranium reduction by Fe (II) in the presence of montmorillonite and nontronite. *Environmental Science & Technology* **2016,** *50*, (15), 8223-8230.
13. Stucki, J. W.; Golden, D.; Roth, C. B., Preparation and handling of dithionite-reduced smectite suspensions. *Clays and Clay Minerals* **1984,** *32*, 191-197.
14. Gorski, C. A.; Aeschbacher, M.; Soltermann, D.; Voegelin, A.; Baeyens, B.; Marques Fernandes, M.; Hofstetter, T. B.; Sander, M., Redox Properties of Structural Fe in Clay Minerals. 1. Electrochemical Quantification of Electron-Donating and -Accepting Capacities of Smectites. *Environmental Science & Technology* **2012,** *46*, (17), 9360-9368.
15. Jones, A. M.; Murphy, C. A.; Waite, T. D.; Collins, R. N., Fe(II) Interactions with Smectites: Temporal Changes in Redox Reactivity and the Formation of Green Rust. *Environmental Science & Technology* **2017,** *51*, (21), 12573-12582.
16. Manceau, A.; Drits, V.; Lanson, B.; Chateigner, D.; Wu, J.; Huo, D.; Gates, W. P.; Stucki, J., Oxidation-reduction mechanism of iron in dioctahedral smectites: II. Crystal chemistry of reduced Garfield nontronite. *American Mineralogist* **2000,** *85*, (1), 153-172.
17. Favre, F.; Stucki, J. W.; Boivin, P., Redox properties of structural Fe in ferruginous smectite. A discussion of the standard potential and its environmental implications. *Clays and clay minerals* **2006,** *54*, (4), 466-472.
18. Neumann, A.; Sander, M.; Hofstetter, T. B., Redox Properties of Structural Fe in Smectite Clay Minerals. In *Aquatic Redox Chemistry*, American Chemical Society: 2011; Vol. 1071, pp 361-379.
19. Bergaya, F.; Lagaly, G., General introduction: clays, clay minerals, and clay science. *Developments in clay science* **2006,** *1*, 1-18.
20. Bergaya, F.; Lagaly, G., *Handbook of clay science*. Newnes: 2013.
21. Gorski, C. A.; Klüpfel, L.; Voegelin, A.; Sander, M.; Hofstetter, T. B., Redox Properties of Structural Fe in Clay Minerals. 2. Electrochemical and Spectroscopic Characterization of Electron Transfer Irreversibility in Ferruginous Smectite, SWa-1. *Environmental Science & Technology* **2012,** *46*, (17), 9369-9377.
22. Gorski, C. A.; Klüpfel, L. E.; Voegelin, A.; Sander, M.; Hofstetter, T. B., Redox Properties of Structural Fe in Clay Minerals: 3. Relationships between Smectite Redox and Structural Properties. *Environmental Science & Technology* **2013,** *47*, (23), 13477-13485.

23. Aeppli, M.; Voegelin, A.; Gorski, C. A.; Hofstetter, T. B.; Sander, M., Mediated Electrochemical Reduction of Iron (Oxyhydr-)Oxides under Defined Thermodynamic Boundary Conditions. *Environmental Science & Technology* **2018,** *52*, (2), 560-570.
24. Aeppli, M.; Kaegi, R.; Kretzschmar, R.; Voegelin, A.; Hofstetter, T. B.; Sander, M., Electrochemical Analysis of Changes in Iron Oxide Reducibility during Abiotic Ferrihydrite Transformation into Goethite and Magnetite. *Environmental Science & Technology* **2019,** *53*, (7), 3568-3578.
25. Gorski, C. A.; Edwards, R.; Sander, M.; Hofstetter, T. B.; Stewart, S. M., Thermodynamic Characterization of Iron Oxide–Aqueous Fe2+ Redox Couples. *Environmental Science & Technology* **2016,** *50*, (16), 8538-8547.
26. Stewart, S. M.; Hofstetter, T. B.; Joshi, P.; Gorski, C. A., Linking Thermodynamics to Pollutant Reduction Kinetics by Fe2+ Bound to Iron Oxides. *Environmental Science & Technology* **2018,** *52*, (10), 5600-5609.
27. Amonette, J. E., Iron redox chemistry of clays and oxides: environmental applications. **2002**.
28. Robinson, T. C.; Latta, D. E.; Leddy, J.; Scherer, M. M., Redox Potentials of Magnetite Suspensions under Reducing Conditions. *Environmental Science & Technology* **2022,** *56*, (23), 17454-17461.
29. Fultz, M. L.; Durst, R. A., Mediator compounds for the electrochemical study of biological redox systems: a compilation. *Analytica Chimica Acta* **1982,** *140*, (1), 1-18.
30. Aeschbacher, M.; Sander, M.; Schwarzenbach, R. P., Novel Electrochemical Approach to Assess the Redox Properties of Humic Substances. *Environmental Science & Technology* **2010,** *44*, (1), 87-93.
31. Vitins, G.; West, K., Lithium Intercalation into Layered LiMnO2. *Journal of The Electrochemical Society* **1997,** *144*, (8), 2587.
32. Malik, M. A.; Kulesza, P. J.; Marassi, R.; Nobili, F.; Miecznikowski, K.; Zamponi, S., Countercation intercalation and kinetics of charge transport during redox reactions of nickel hexacyanoferrate. *Electrochimica Acta* **2004,** *49*, (25), 4253-4258.
33. Aurbach, D.; Levi, M. D.; Levi, E., A review on the solid-state ionics of electrochemical intercalation processes: How to interpret properly their electrochemical response. *Solid State Ionics* **2008,** *179*, (21), 742-751.
34. Levi, M. D.; Aurbach, D., Frumkin intercalation isotherm — a tool for the description of lithium insertion into host materials: a review. *Electrochimica Acta* **1999,** *45*, (1), 167-185.
35. Hurlbutt, K.; Wheeler, S.; Capone, I.; Pasta, M., Prussian Blue Analogs as Battery Materials. *Joule* **2018,** *2*, (10), 1950-1960.
36. Moritomo, Y.; Takachi, M.; Kurihara, Y.; Matsuda, T., Thin film electrodes of Prussian blue analogues with rapid Li+ intercalation. *Applied Physics Express* **2012,** *5*, (4), 041801.
37. Heubner, C.; Schneider, M.; Michaelis, A., Investigation of charge transfer kinetics of Li-Intercalation in LiFePO4. *Journal of Power Sources* **2015,** *288*, 115-120.
38. Yun, J.; Pfisterer, J.; Bandarenka, A. S., How simple are the models of Na intercalation in aqueous media? *Energy & Environmental Science* **2016,** *9*, (3), 955-961.

39. Porada, S.; Shrivastava, A.; Bukowska, P.; Biesheuvel, P. M.; Smith, K. C., Nickel Hexacyanoferrate Electrodes for Continuous Cation Intercalation Desalination of Brackish Water. *Electrochimica Acta* **2017,** *255*, 369-378.
40. Singh, K.; Qian, Z.; Biesheuvel, P. M.; Zuilhof, H.; Porada, S.; de Smet, L. C. P. M., Nickel hexacyanoferrate electrodes for high mono/divalent ion-selectivity in capacitive deionization. *Desalination* **2020,** *481*, 114346.
41. Neff, V. D., Electrochemical Oxidation and Reduction of Thin Films of Prussian Blue. *Journal of The Electrochemical Society* **1978,** *125*, (6), 886.
42. Itaya, K.; Uchida, I.; Neff, V. D., Electrochemistry of polynuclear transition metal cyanides: Prussian blue and its analogues. *Accounts of Chemical Research* **1986,** *19*, (6), 162-168.
43. Liu, T.; Pell, W. G.; Conway, B. E., Self-discharge and potential recovery phenomena at thermally and electrochemically prepared RuO2 supercapacitor electrodes. *Electrochimica Acta* **1997,** *42*, (23), 3541-3552.
44. Newman, J.; Balsara, N. P., *Electrochemical systems*. John Wiley & Sons: 2021.
45. Thomas, K. E.; Newman, J.; Darling, R. M., Mathematical modeling of lithium batteries. In *Advances in lithium-ion batteries*, Springer: 2002; pp 345-392.
46. Li, B.; Assat, G.; Pearce, P. E.; Nikitina, V. A.; Iadecola, A.; Delacourt, C.; Tarascon, J.-M., Exploring the Kinetic Limitations Causing Unusual Low-Voltage Li Reinsertion in Either Layered or Tridimensional Li2IrO3 Cathode Materials. *Chemistry of Materials* **2020,** *32*, (5), 2133-2147.
47. Li, B.; Sougrati, M. T.; Rousse, G.; Morozov, A. V.; Dedryvère, R.; Iadecola, A.; Senyshyn, A.; Zhang, L.; Abakumov, A. M.; Doublet, M.-L.; Tarascon, J.-M., Correlating ligand-to-metal charge transfer with voltage hysteresis in a Li-rich rock-salt compound exhibiting anionic redox. *Nature Chemistry* **2021,** *13*, (11), 1070-1080.
48. Pothanamkandathil, V.; Boualavong, J.; Gorski, C. A., Open-Circuit Potential Drift in Intercalation Electrodes: Role of Charge Redistribution in a Prussian Blue Analog. *Journal of The Electrochemical Society* **2023,** *170*, (11), 110503.
49. Rothwell, K. A.; Pentrak, M. P.; Pentrak, L. A.; Stucki, J. W.; Neumann, A., Reduction Pathway-Dependent Formation of Reactive Fe(II) Sites in Clay Minerals. *Environmental Science & Technology* **2023,** *57*, (28), 10231-10241.
50. Yuan, S.; Liu, X.; Liao, W.; Zhang, P.; Wang, X.; Tong, M., Mechanisms of electron transfer from structrual Fe(II) in reduced nontronite to oxygen for production of hydroxyl radicals. *Geochimica et Cosmochimica Acta* **2018,** *223*, 422-436.
51. Liao, W.; Yuan, S.; Liu, X.; Tong, M., Anoxic storage regenerates reactive Fe (II) in reduced nontronite with short-term oxidation. *Geochimica et Cosmochimica Acta* **2019,** *257*, 96-109.
52. Singh, K.; Bouwmeester, H. J. M.; de Smet, L. C. P. M.; Bazant, M. Z.; Biesheuvel, P. M., Theory of Water Desalination with Intercalation Materials. *Physical Review Applied* **2018,** *9*, (6), 064036.
53. Malaie, K.; Scholz, F.; Schröder, U., A thermodynamic model for the insertion electrochemistry of battery cathodes. *ChemElectroChem* **2023,** *10*, (7), e202201118.

54. Neumann, A.; Olson, T. L.; Scherer, M. M., Spectroscopic evidence for Fe (II)–Fe (III) electron transfer at clay mineral edge and basal sites. *Environmental science & technology* **2013,** *47*, (13), 6969-6977.
55. Fick, A., V. On liquid diffusion. *The London, Edinburgh, and Dublin Philosophical Magazine and Journal of Science* **1855,** *10*, (63), 30-39.
56. Sander, M.; Hofstetter, T. B.; Gorski, C. A., Electrochemical Analyses of Redox-Active Iron Minerals: A Review of Nonmediated and Mediated Approaches. *Environmental Science & Technology* **2015,** *49*, (10), 5862-5878.
57. Aeppli, M.; Giroud, S.; Vranic, S.; Voegelin, A.; Hofstetter, T. B.; Sander, M., Thermodynamic controls on rates of iron oxide reduction by extracellular electron shuttles. *Proceedings of the National Academy of Sciences* **2022,** *119*, (3), e2115629119.
58. Tournassat, C.; Greneche, J.-M.; Tisserand, D.; Charlet, L., The titration of clay minerals: I. Discontinuous backtitration technique combined with CEC measurements. *Journal of Colloid and Interface Science* **2004,** *273*, (1), 224-233.
59. Sposito, G., *The thermodynamics of soil solutions*. 1981.
60. Bard, A. J.; Faulkner, L. R.; White, H. S., *Electrochemical methods: fundamentals and applications*. John Wiley & Sons: 2022.
61. Gellings, P. J., *Handbook of solid state electrochemistry*. CRC press: 2019.
62. Bruce, P. G., *Solid state electrochemistry*. Cambridge university press: 1997.
63. Yuan, S.; Liu, X.; Liao, W.; Zhang, P.; Wang, X.; Tong, M., Mechanisms of electron transfer from structrual Fe (II) in reduced nontronite to oxygen for production of hydroxyl radicals. *Geochimica et Cosmochimica Acta* **2018,** *223*, 422-436.
64. Peerce, P. J.; Bard, A. J., Polymer films on electrodes: Part III. Digital simulation model for cyclic voltammetry of electroactive polymer film and electrochemistry of poly(vinylferrocene) on platinum. *Journal of Electroanalytical Chemistry and Interfacial Electrochemistry* **1980,** *114*, (1), 89-115.
65. Ostrogorsky, A. G.; Glicksman, M. E., 25 - Segregation and Component Distribution. In *Handbook of Crystal Growth (Second Edition)*, Rudolph, P., Ed. Elsevier: Boston, 2015; pp 995-1047.
66. Neumann, A.; Petit, S.; Hofstetter, T. B., Evaluation of redox-active iron sites in smectites using middle and near infrared spectroscopy. *Geochimica et Cosmochimica Acta* **2011,** *75*, (9), 2336-2355.
67. Taylor, H. P.; O'Neil, J. R.; Kaplan, I. R., Stable isotope geochemistry: A tribute to Samuel Epstein. *(No Title)* **1991**.
68. Xue-lei, C.; Ohmoto, H., Kinetics of isotope exchange reactions involving intra- and intermolecular reactions: I. Rate law for a system with two chemical compounds and three exchangeable atoms. *Geochimica et Cosmochimica Acta* **1991,** *55*, (7), 1953-1961.
69. Neumann, A.; Wu, L.; Li, W.; Beard, B. L.; Johnson, C. M.; Rosso, K. M.; Frierdich, A. J.; Scherer, M. M., Atom Exchange between Aqueous Fe(II) and Structural Fe in Clay Minerals. *Environmental Science & Technology* **2015,** *49*, (5), 2786-2795.

70. Alexandrov, V.; Neumann, A.; Scherer, M. M.; Rosso, K. M., Electron Exchange and Conduction in Nontronite from First-Principles. *The Journal of Physical Chemistry C* **2013,** *117*, (5), 2032-2040.
71. Peiffer, S.; Kappler, A.; Haderlein, S. B.; Schmidt, C.; Byrne, J. M.; Kleindienst, S.; Vogt, C.; Richnow, H. H.; Obst, M.; Angenent, L. T.; Bryce, C.; McCammon, C.; Planer-Friedrich, B., A biogeochemical–hydrological framework for the role of redox-active compounds in aquatic systems. *Nature Geoscience* **2021,** *14*, (5), 264-272.
72. Ginn, B.; Meile, C.; Wilmoth, J.; Tang, Y.; Thompson, A., Rapid Iron Reduction Rates Are Stimulated by High-Amplitude Redox Fluctuations in a Tropical Forest Soil. *Environmental Science & Technology* **2017,** *51*, (6), 3250-3259.
73. Zhao, G.; Tan, M.; Wu, B.; Zheng, X.; Xiong, R.; Chen, B.; Kappler, A.; Chu, C., Redox Oscillations Activate Thermodynamically Stable Iron Minerals for Enhanced Reactive Oxygen Species Production. *Environmental Science & Technology* **2023,** *57*, (23), 8628-8637.
74. Pentráková, L.; Su, K.; Pentrák, M.; Stucki, J. W., A review of microbial redox interactions with structural Fe in clay minerals. *Clay Minerals* **2013,** *48*, (3), 543-560.